Despite several pharmacological applications, only few lanthanide – hydrazones complexes are investigated for their DNA-binding. Thus there is much need to investigate DNA binding ability of lanthanide complexes of hydrazones to showcase their biological applications. In the light of applications [1-4] and objectives, lanthanide [Ce(III), Pr(III), Nd(III) and Sm(III)] complexes with 2-benzoylpyridine benzoyl hydrazone (BPBH) are synthesized characterized based on physico-chemical techniques and spectral methods viz., IR, UV-Visible spectroscopy. Electrochemical properties of all complexes are studied by cyclic voltammetry. Binding interactions of metal complexes with calf-thymus DNA are carried out using absorption spectroscopy. DNA cleavage activities of the complexes are investigated using gel electrophoresis experiments. The structure of cerium complex is determined using single crystal X-Ray diffraction studies. The structural characterization of 12-coordinate cerium(III) complex with BPBH is a major highlight in this Chapter. Synthesis and characterization of BPBH (Fig 8.1) are given in Chapter 2. The ligand is synthesized by using corresponding precursors.

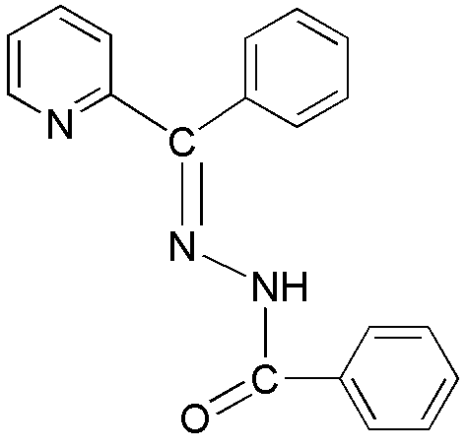

Fig 8.1: The structure of BPBH

a. Physico-chemical properties:

Syntheses of lanthanide(III) complexes are given in Chapter-2 (Section 2 iii). All the complexes are stable at room temperature, non-hygroscopic, less soluble in water, methanol, ethanol readily soluble in DMF and DMSO. The analytical data are consistent with the proposed molecular formulae of complexes. Physical properties viz., colour of the complex, melting points and percentage of yield are given in **Table 8.1.**

b. Conductivity measurements

All the complexes are freely soluble in dimethylformamide (DMF), hence the solutions of these metal complexes were prepared in DMF to perform conductivity measurements. Milli-molar solutions (10^{-3}M) were prepared in 25-ml standard flasks by dissolving the metal complex in DMF and then the solutions were transferred into clean dry 100-ml beakers. Conductivity values of the solutions were measured at room temperature. The molar conductivity values (6.8-19.1 $\Omega^{-1}cm^2$ mol^{-1}) for the complexes suggest that these are non-electrolytes [5].

Table 8.1. Colors, analytical data, molar conductivities and M. P of the BPBH ligand and its Lanthanide(III) complexes

Compound	**Colour**	**M.P °C**	**Yield %**	**Found (cal %)**			**Λm[a]**
				C	**H**	**N**	
BPBH	White	140-142	71	76.70 (75.72)	4.99 (5.01)	13.97 (13.94)	…
$[La(BPBH)_2(NO_3)_3]$	White	228-230	68	49.12 (49.25)	3.35 (3.26)	13.54 (13.60)	12.5
$[Ce(BPBH)_2(NO_3)_3]$	Yellow	225-227	69	49.43 (49.25)	3.36 (3.26)	13.65 (13.59)	13.4
$[Pr(BPBH)_2(NO_3)_3]$	Light Green	208-210	71	49.25 (49.15)	3.34 (3.25)	13.45 (13.57)	10.6
$[Nd(BPBH)_2(NO_3)_3]$	Light Pink	222-224	72	48.84 (48.97)	3.63 (3.24)	1362 (13.53)	19.1
$[Sm(BPBH)_2(NO_3)_3]$	white	202-204	60	48.64 (48.65)	3.20 (3.22)	13.46 (13.44)	6.8

[a] $(\Omega^{-1}\ cm^2\ mol^{-1})$

c. Electronic spectra

Electronic spectrum of the free ligand in UV region shows an intense band at 295 nm and weaker band at 367 nm which are assigned to the π–π* and n–π*transitions respectively. These are slightly, shifted to higher or lower energy levels in absorption spectra of the lanthanide complexes. In visible region the electronic spectrum of Pr(III), Nd(III), Sm(III) complexes show several important f-f spectral bands, shown in Fig.8.2. The electronic spectra of the lanthanide complexes in the visible region exhibits generally red shift of all the f-f spectral bands relative to the corresponding Ln(III) aquo ion, shown in Fig. 8.3. The shifts have been attributed by Jorgenson to the effective crystal field upon inter electronic repulsion between the 4f electons and is related to covalence in the metal-ligand bond. The values of the bonding parameters are shown in Table 8.2. The positive and negative values of δ and $b^{1/2}$ for a complex correspond to covalent and ionic characters, respectively. The *nephelauxetic* ratio (β) is less than unity and positive values of Sinha's parameter (δ) and the bonding parameter ($b^{1/2}$) suggest the occurrence of some covalent character in the metal– ligand bond [6, 7]. The small (δ%) values of the complexes indicate weak covalent bonding in the complexes. the small $\mathbf{b}^{½}$ values suggest a small participation of 4f orbital's in bonding.

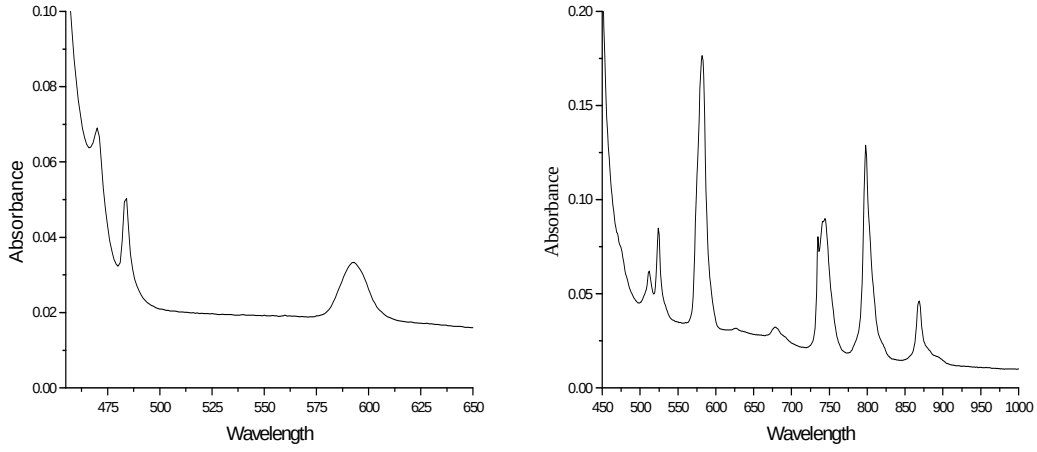

(A) (B)

Fig 8.2: Electronic spectra of (A) Pr complex and (B) Nd complex

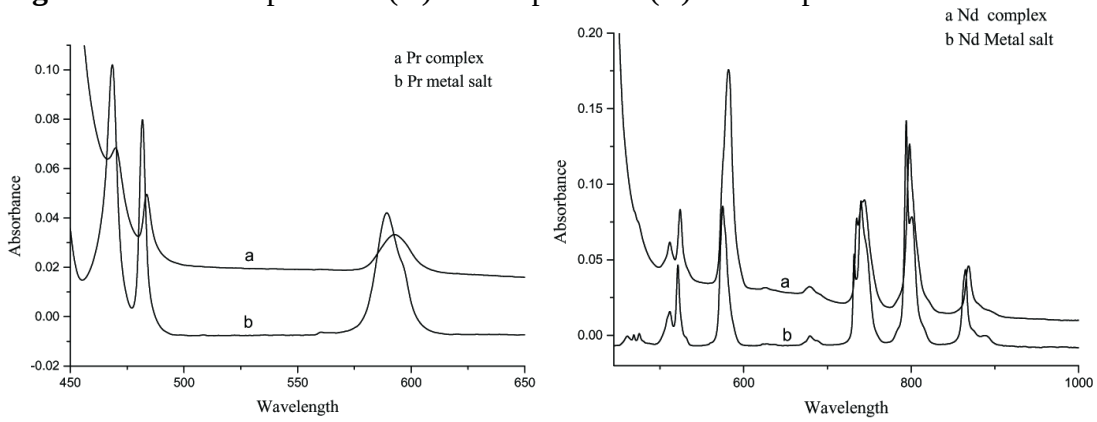

(A) (B)

Fig 8.3: Electronic absorption spectra of (A)$Pr(NO_3)_3.6H_2O$ (red) & [$Pr(BPBH)_2(NO_3)_3$] (black) and (B)$Nd(NO_3)_3.6H_2O$ (red) & [$Nd(BPBH)_2(NO_3)_3$] (black) in the visible region

Table 8.2. Electronic spectral data of the lanthanide complexes and related bonding parameter

Complexes	Frequency (cm^{-1})		Red shift (cm^{-1})	Assignment	Covalent parameter
	Lanthanide Aqua ion	Lanthanide complexes			
$[Pr(BPBH)_2(NO_3)_3]$	16,977	16,863	114	$^3H_4 \rightarrow {}^1D_2$	$\beta = 0.9875$
	20,746	20,661	85	$^3H_4 \rightarrow {}^3P_0$	$\delta\% = 1.26$
	21,367	21,276	91	$^3H_4 \rightarrow {}^3P_1$	$b^{1/2} = 0.079$
	22,522	22,471	51	$^3H_4 \rightarrow {}^3P_2$	$\eta = 0.00633$
$[Nd(BPBH)_2(NO_3)_3]$	11,560	11,520	40	$^4I_{9/2} \rightarrow {}^4F_{3/2}$	$\beta = 0.9957$
	12,594	12,531	63	$^4I_{9/2} \rightarrow {}^4F_{5/2}$	$\delta\% = 0.43$
	13,513	13,495	18	$^4I_{9/2} \rightarrow {}^4F_{7/2}$, $^3S_{3/2}$	$b^{1/2} = 0.046$
	17,391	17,182	209	$^4I_{9/2} \rightarrow {}^4G_{5/2,}$ $^2G_{7/2}$	$\eta = 0.0022$
	19,120	19.083	37	$^4I_{9/2} \rightarrow {}^4G_{7/2}$	
	19,569	19,531	38	$^4I_{9/2} \rightarrow {}^4G_{9/2}$	
$[Sm(BPBH)_2(NO_3)_3]$	24,038	23,980	58	$^6H_{5/2} \rightarrow {}^6P_{5/2}$	$\beta = 0.9988$
	22,675	22,650	25	$^6H_{5/2} \rightarrow {}^4G_{9/2}$	$\delta\% = 0.12$
	21,598	21,593	5	$^6H_{5/2} \rightarrow {}^4I_{13/2}$	$b^{1/2} = 0.024$
	20,876	20,872	4	$^6H_{5/2} \rightarrow {}^4I_{11/2}$	$\eta = 0.0006$
	20,040	20,000	40	$^6H_{5/2} \rightarrow {}^6G_{7/2}$	

d. Infrared Spectra

The FT- IR spectra of complexes in the region 4000-400 cm^{-1} are analyzed in comparison with that of the spectrum of metal free BPBH. The characteristic IR peaks of BPBH and its lanthanide complexes are given in Table 8.3. IR spectra of the five complexes are strikingly similar in relative positions and intensities of the peaks, which suggest a close structural relationship among the compounds. The IR spectrum of free ligand shows a strong band at 1673 cm^{-1}, which is attributable to stretching vibrations of (C=O) group. The vibrational band at 1583 cm^{-1} can be assigned to the *ν*(C=N) of azomethine. In the IR spectra of their lanthanide(III) complexes, the *ν*(C=O) and *ν*(C =N) bands are shifted to lower frequencies by 24–41, 44–73 cm^{-1} respectively. The negative shifts indicate participation of the amido oxygen and azomethine nitrogen in coordination to the metal ion [8]. The vibrational band at 3100 cm^{-1} can be assigned to the *ν*(N-H) for the free ligand. The *ν*(N-H) band is observed in 3197-3211 cm^{-1} region in the spectra of complexes. The observance ν(C=O) and ν(N-H) bands in the IR spectra of complexes indicates that BPBH acts as neutral tridentate ligand in the complex formation. The pyridine ring in-plane deformation mode is observed at 629 cm^{-1} in the spectrum of BPBH. The band is shifted to 630-632 cm^{-1} in the spectra of lanthanide complexes indicating coordination of the heterocyclic aromatic nitrogen [8].

The absorption bands due to the coordinated nitrate groups (*C*2v) are observed at about 1464-1471 cm^{-1} (ν_1), 1300-1302 cm^{-1} (ν_4), 1027-1029 cm^{-1} (ν_2) and 816-819 cm^{-1} (ν_3) for the nitrate complexes. The frequency separation [$\Delta\nu = \nu_1 - \nu_4$] between the asymmetric and symmetric stretching of this group can be made to distinction

between these binding states. The separation between two bands is between 162–171 cm^{-1}, which shows the presence of bidentate nitrates [9, 10] in complexes. The vibrational band is absent at 1384 cm^{-1} in IR spectra of complexes indicating the absence of ionic nitrate (D_{3h} symmetry), which is in agreement with the results of the conductivity experiments. The new bands in 416 -423 and 541 - 546 cm^{-1} regions are assigned to ν(Ln–O) and ν(Ln–N) vibration respectively. IR Spectra of $[Ce(BPBH)_2(NO_3)_3]$ complex is shown in Fig 8.4

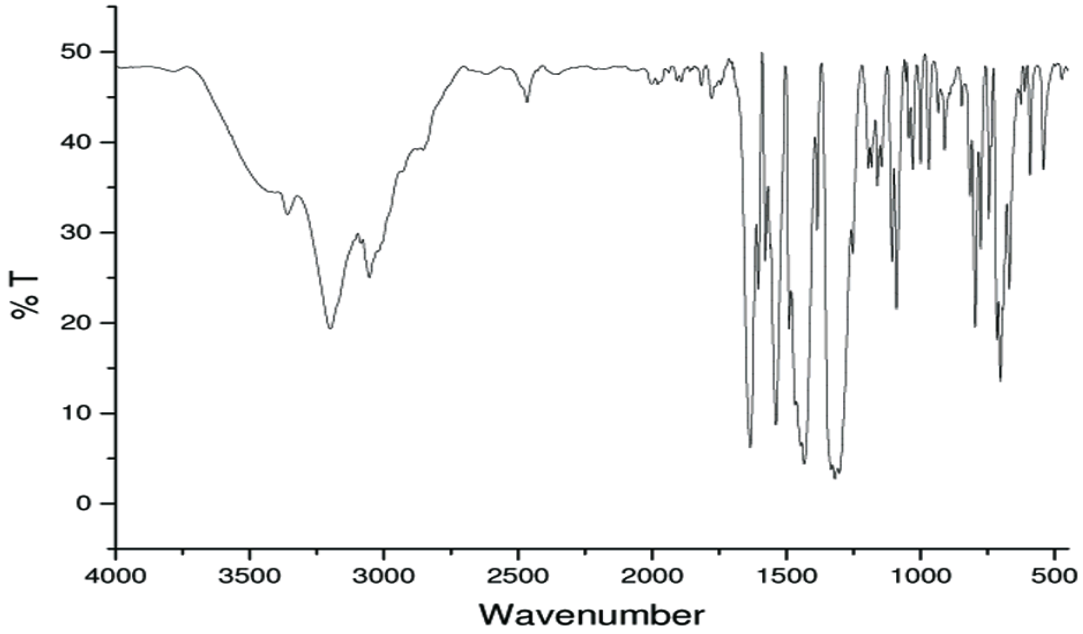

Fig 8.4: IR Spectra of $[Ce(BPBH)_2(NO_3)_3]$ complex in KBr Disc

Table 8.3. Infrared spectral data(cm^{-1}) for the BPBH ligand and its lanthanide(III) complexes

Compound	**ν(N-H)**	**ν(C=O)**	**ν(C=N)**	**ν(NO_3^-)**				
				$\nu_1(NO_3^-)$	**$\nu_4(NO_3^-)$**	**$\nu_2(NO_3^-)$**	**$\nu_3(NO_3^-)$**	**ν_1-ν_4**
BPBH	3122	1673	1583	…	…	…	…	…
$[La(BPBH)_2(NO_3)_3]$	3168	1634	1534	1470	1301	1027	819	169
$[Ce(BPBH)_2(NO_3)_3]$	3192	1632	1536	1471	1300	1027	815	171
$[Pr(BPBH)_2(NO_3)_3]$	3214	1636	1535	1470	1301	1028	817	169
$[Nd(BPBH)_2(NO_3)_3]$	3201	1636	1532	1468	1302	1029	818	166
$[Sm(BPBH)_2(NO_3)_3]$	3196	1649	1535	1464	1302	1028	816	162

e. Thermal analysis

Thermogravimetric (TG) and differential thermal analysis of BPBH ligand and corresponding lanthanide complexes were carried out within the temperature range from ambient temperature up to 800 ºC under a nitrogen flow with heating rate 10°C/min.

All the complexes showed similar thermal decomposition Fig. 8.5. The TGA curve of Ce(III) complex undergoes two-stage changes. All Ln(III) complexes are thermally stable up to 240 ºC indicting absence of lattice or coordinated water and solvent molecules. The first stage of decomposition in the range 235-240 ºC is due to loss of three nitrate ions and one ligand moiety with a weight loss of 52.57% which is consistent with theoretical value (52.54%). The second stage of decomposition in the range 241- 800 ºC corresponds to the elimination and/or decomposition of bound remaining ligand [11].

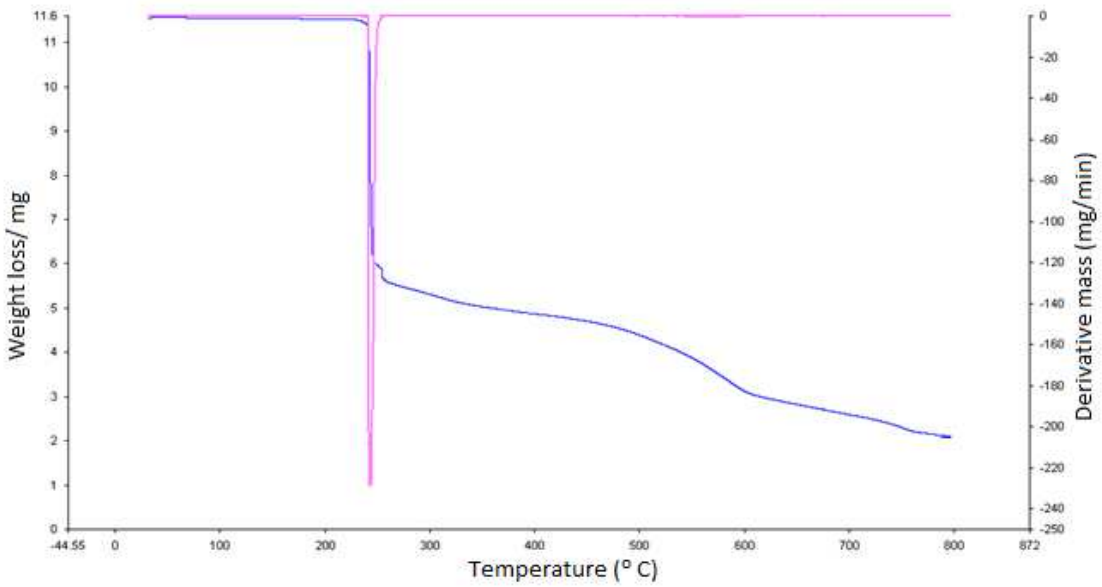

Fig 8.5: TG and DTG curves for $[Ce(BPBH)_2(NO_3)_3]$

f. Description of Crystal structure of [Ce(BPBH)$_2$(NO$_3$)$_3$]

The [Ce(BPBH)$_2$(NO$_3$)$_3$] compound crystallizees in, monoclinic space group C2/c and the structure contains six neutral [Ce(BPBH)$_2$(NO$_3$)$_3$] molecules in each unit cell shown in Fig. 8.6 Crystal data and structure refinement parameters are shown in Table 8.4. Selected bond lengths and bond angles are given in Tables 8.5. ORTEP view of [Ce(BPBH)$_2$(NO$_3$)$_3$] together with the atom labeling scheme is used shown in Fig. 8.7 Cerium metal atom is surrounded by 12 coordinated donor atoms. Six of them belong to two neutral tridentate ligands and six from the three bidentate nitrate groups. The BPBH ligand is coordinated to central metal atom to form two five membered rings. One five-membered chelate ring involves the pyridine nitrogen and the azomethine nitrogen and another five-membered chelate ring involves the azomethine nitrogen and carbonyl oxygen donor atoms.

Generally, for 12 coordinate complexes six polyhedra are considered [12]. They are (i)icosahedron, (ii)cuboctahedron, (iii)anti cuboctahedron, (iv)hexagonal prism, (v)hexagonal antiprism and (vi) Bicapped pentagonal prism. [Ce(BPBH)$_2$(NO$_3$)$_3$] shows that the geometry of 12-coordination is distorted icosahedron in which five triangles are joined at each vertex. There are 30 edges, 12 vertices and 20 faces (i.e., V – E + F = 2, Euler's formula, 12-30+ 20 = 2). In our case the coordination polyhedron around **cerium** atom is distorted icosahedron and is shown in Fig. 8.8.

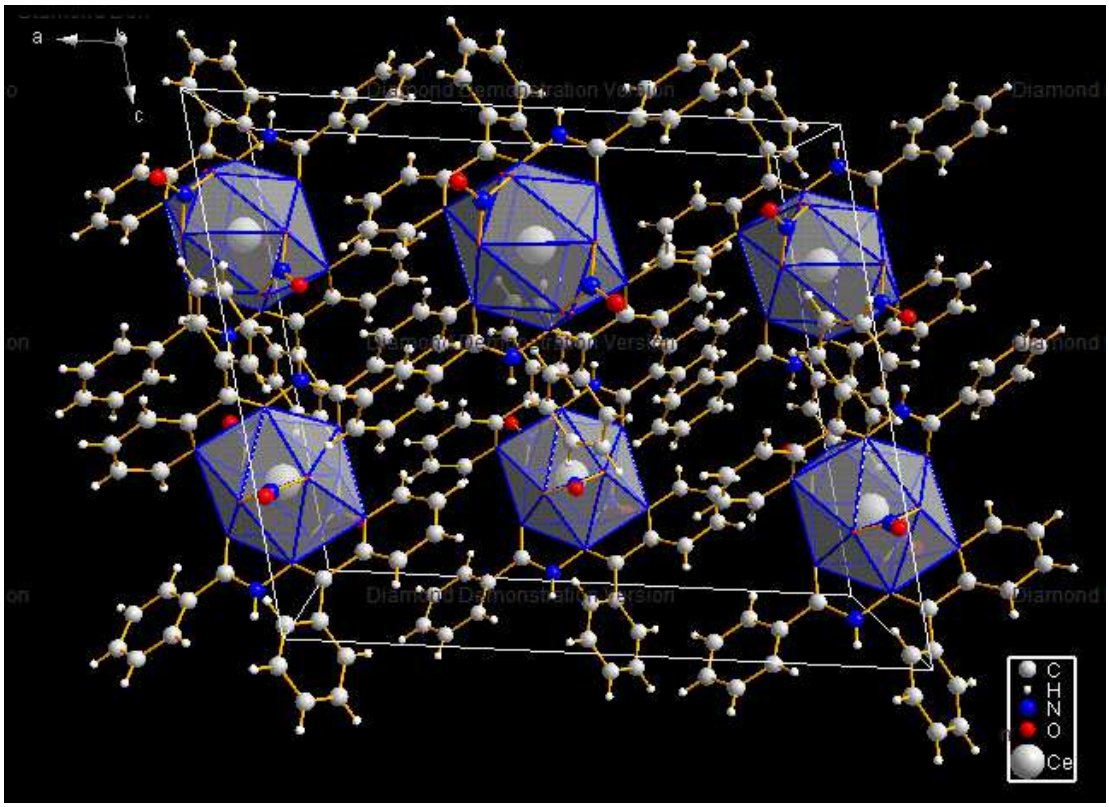

Fig 8.6: Unit cell structure of $[Ce(BPBH)_2(NO_3)_3]$ with distorted icosahedrons around Ce(III) centers

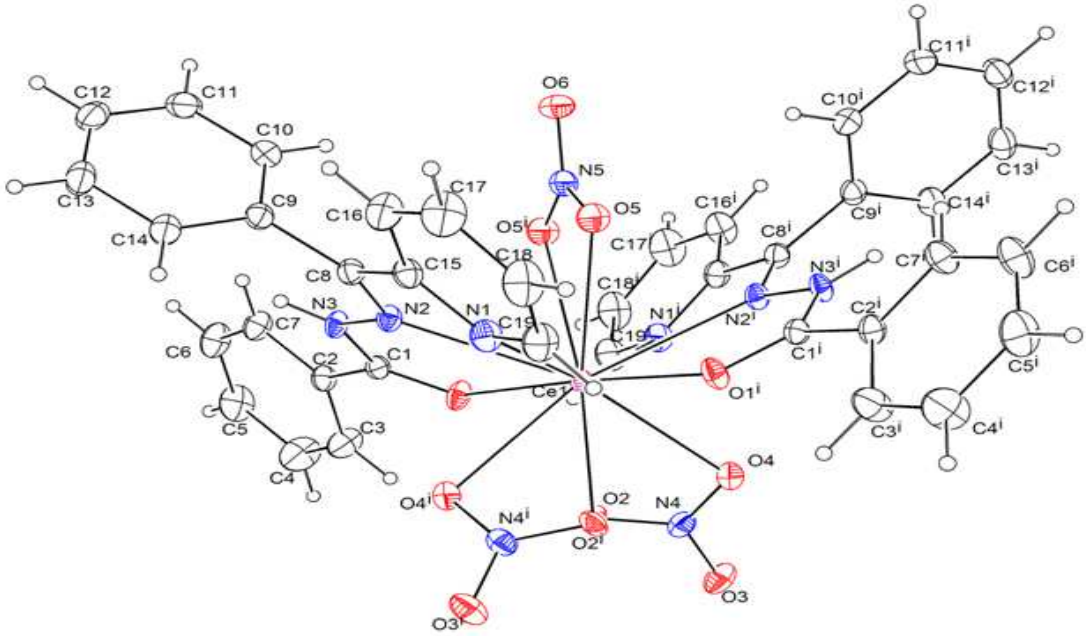

Fig 8.7: ORTEP view showing molecular structure of $[Ce(BPBH)_2(NO_3)_3]$ complex

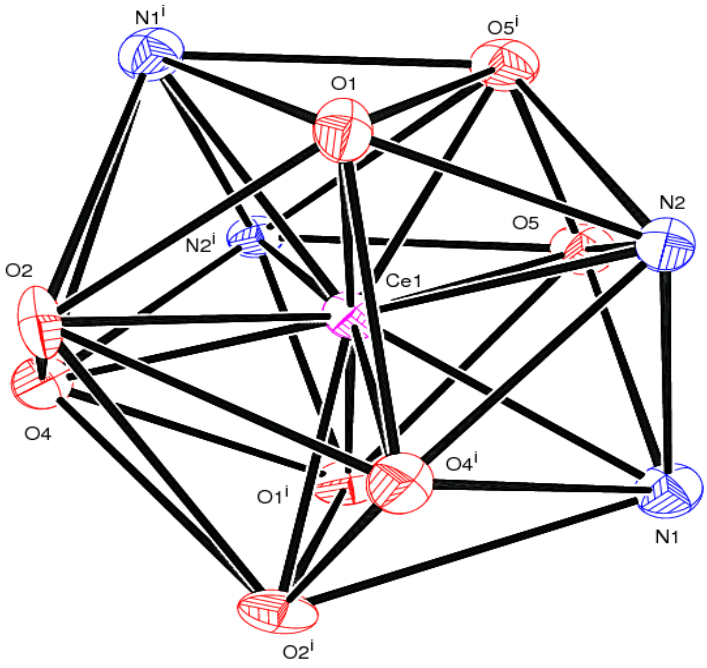

Fig 8.8: The coordination polyhedron (Distorted Icosahedron) around Cerium(III) ion in 12- coordinate $[Ce(BPBH)_2(NO_3)_3]$ complex

The phenyl rings adjacent to the 2-pyridyl ring are twisted out of this plane so as to avoid H-H repulsion with the proton in the 3-position of the pyridyl ring. The Ce-O bond distances [2.4952(12) to 2.72(2)] are shorter than Ce-N [2.9365(16) to 2.7706(14)] as can expected for a hard oxygen donor bounded to a lanthanide ion [13].

The Ce-N(py) distance is 2.9365(16) and Ce-N (azo) distance is 2.7706(14) . the difference may arise from constraints involved in chelate-ring formation or from the differing positions in which N(py) and N(azo) occupy in the coordination polyhedron, as well as from differential Ce → N back donation [14]. Cerium to donor atom bond length order is given below.

Ce-N(pyridine) > Ce-N(azomethine) > Ce-O(Amide carbonyl) > Ce-O(Nitrate).

Table 8.4. Crystal data and structure refinement parameters for $[Ce(BPBH)_2(NO_3)_3]$

Empirical formula	C38 H30 Ce N9 O11
Formula weight (g mol^{-1})	928.83
Temperature (K)	293(2)
Wavelength (Å)	0.71073
Crystal system	Monoclinic
space group	*C2/c*
Unit cell dimensions	
a (Å)	18.5544(5)
b (Å)	13.5066(4)
c (Å)	16.1009(4)
α (°)	90
β (°)	102.9450(10)
γ (°)	90
Volume ($Å^3$)	3932.45(19)
Z	4
Calculated density ($mg.m^{-3}$)	1.569
Absorption coefficient (mm^{-1})	1.230
F (000)	1868
Crystal size (mm)	0.30 x 0.20 x 0.20
θ range for data collection (°)	2.25 - 24.99
Limiting indices	$-22 \leq h \leq 22$, $-15 \leq k \leq 16$, $-12 \leq l \leq 19$
Reflections collected	17721
Unique	3449 [R_{int} = 0.0283]
Completeness to θ (%)	99.8
Absorption correction	Semi-empirical from equivalents
Max. And min. transmission	0.7995 and 0.7036
Refinement method	Full-matrix least-squares on F^2
Data / restraints / parameters	3449 / 56 / 298
Goodness-of-fit on F^2	1.071
Final *R* indices [$I > 2\sigma(I)$]	*R1* = 0.0183, w*R2* = 0.0436
R indices (all data)	*R1* = 0.0199, w*R2* = 0.0443
Largest diff. peak and hole (e $Å^{-3}$)	0.420 and -0.219

Table 8.5. Selected bond lengths (Å) and angles (°) of $[Ce(BPBH)_2(NO_3)_3]$

Bond lengths (Å)			
N(1)-Ce(1)	2.9365(16)	N(2)-Ce(1)	2.7706(14)
O(1)-Ce(1)	2.4952(12)	O(5)-Ce(1)	2.6808(14)
Ce(1)-O(2)	2.72(2)	Ce(1)-O(4)	2.62(2)
Bond Angles (°)			
O(1)#1-Ce(1)-O(1)	176.89(6)	O(4)#1-Ce(1)-O(4)	101.6(9)
O(2)#1-Ce(1)-O(2)	71.5(6)	O(4)-Ce(1)-O(2)#1	68.8(5)
O(4)#1-Ce(1)-O(2)#1	48.4(5)	O(5)-Ce(1)-O(5)#1	46.98(6)

Three nitrates have metal to ligand bond angels are nearly same but bond lengths are different. Based on bond lengths three nitrate have two type of coordination, one type of two nitrates bond lengths are unsymmetrical [2.72(2), 2.62(2)], another type of nitrate bond lengths are symmetrical [2.6808(14)].

The bond lengths of [C(1)-O(1)] 1.231(2), [C(1)-N(3)] 1.338(2) are compared with [C-O (1.43 Å), C=O (1.20 Å), C-N (1.47 Å), C=N (1.27 Å)] suggesting an keto form only in coordination mode. It is well known that pyridine based hydrazones can exist as two geometrical isomers based on azomethine, syn (Z) and anti (E) shown in Fig 8.9, but in our case, only the E isomer is possible in the cerium complex. The torsion angles are C15–C8–N2–N3(173.53°), N2–N3–C1–O1(-4.45°), observed supports the hydrazone E conformation in coordination[15].

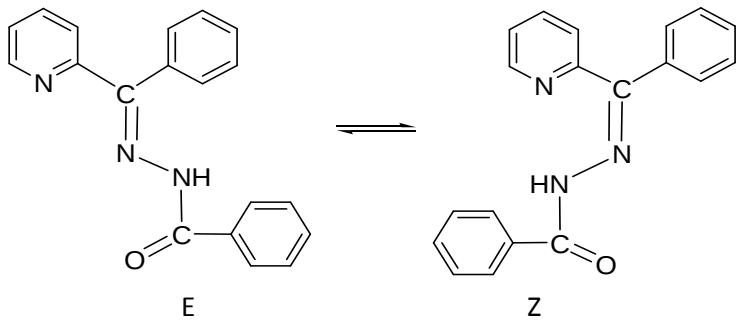

E Z

Fig 8.9: Geometrical isomers of 2-benzoylpyridine benzhydrazone

The intra-molecular C–H…π interaction between the phenyl ring (adjacent to the 2-pyridyl ring) and pyridine hydrogen shows a distance of 3.364 Å. The intra-molecular N–H…π interaction between the phenyl ring (adjacent to the 2-pyridyl ring) and imine hydrogen shows a distance of 3.036 Å. X-H…π intra molecular interactions for the Cerium complex as shown in Fig 8.10

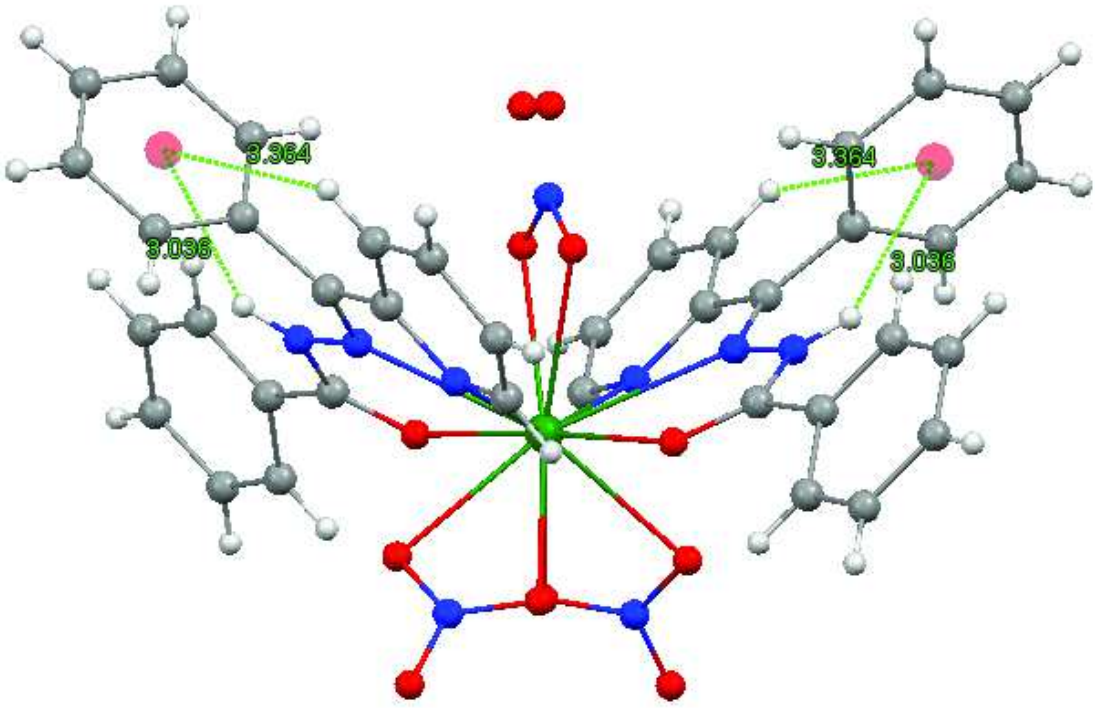

Fig 8.10: X-H…π intra molecular interactions for the Cerium complex

Another interesting feature of the $[Ce(BPBH)_2(NO_3)_3]$ complex is the presence of nitrate…π and XH…π interactions (Fig. 8.11 and Fig. 8.12). $O_{(nitrate)}$ … π edge-to-face interactions are present between oxygen atom of nitrate group and phenyl with O…π distance of 3.007 Å for N(4)-O(3)... Cg(I) [Cg(I) is centroid for C(9)/C(14) ring] (Fig. 8.11). Also, in the crystal packing CH…π interactions are exist between the hydrogen atom of phenyl ring (2-benzoyl) and phenyl ring (2-benzoyl)of neighbor

molecule, with CH…π distance of 3.576 Å for C(11)-H(12)... Cg(I) [Cg(1) is centroid for C(9)/C(14) ring] (Fig. 8.12). Details of Intra and Inter molecular are given in Table 8.6.

In the cerium complex mainly N–H···O type of strong intermolecular hydrogen bonds are present between the imine nitrogen and the oxygen atom (not involved in bond formation with metal) of coordinate nitrate ion. View of the hydrogen bond network of $[Ce(BPBH)_2(NO_3)_3]$ complex is shown in Fig. 8.13. Selected hydrogen bond lengths and angles are listed in Table 8.7.

The complex is well stabilized due to presence of intra-molecular X–H…π interactions, intermolecular π – π, niitrate…π interactions and Hydrogen bonding.

Table 8.6. X-H…π and Nitrate…π interactions for the Cerium complex

D-H...A	**d(H...A)**	**d(D...A)**	**<(DHA)**
Intramolecular X-H…π interactions			
C(16)-H(17)…Cg(I)	3.364	3.968	124.68
N(3)-H(3A)... Cg(I)	3.036	3.635	128.62
Intermolecular C-H…π interactions			
C(11)-H(12)…Cg(I)	3.576	4.183	125.26
Nitrate….π interactions			
N(4)-O(3)... Cg(I)	3.007	3.558	106.61

Cg(I) = C9-C14 ring

Table 8.7. Hydrogen bonds (Å) and Angles (˚) for the Cerium complex

D-H...A	**d(D-H)**	**d(H...A)**	**d(D...A)**	**<(DHA)**
N(3)-H(3A)...O(3)[a]	0.86	2.23	3.033(2)	154.5

[a]Symmetry transformations used to generate equivalent atoms: x,-y+1,z-1/

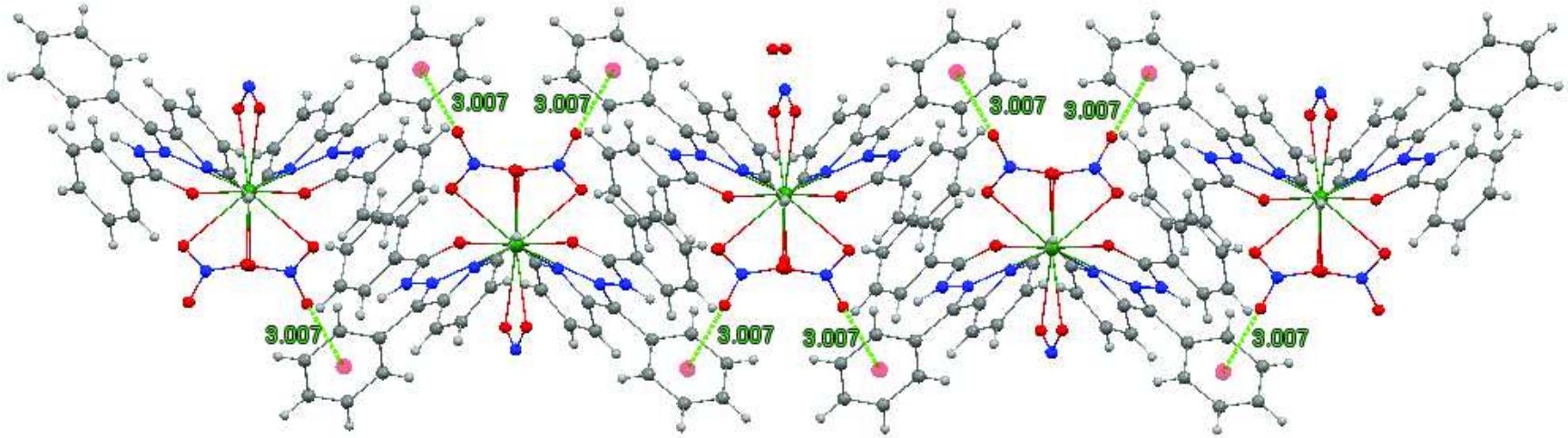

Fig 8.11. Inter molecular Nitrate – π interactions of $[Ce(BPBH)_2(NO_3)_3]$

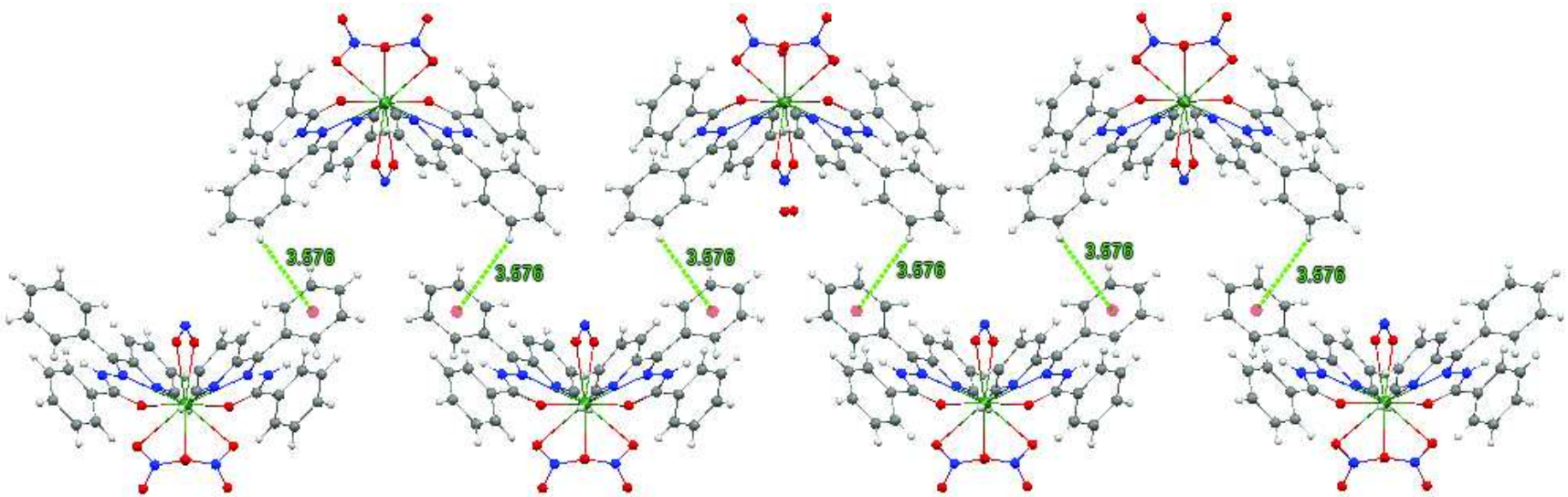

Fig 8.12: Inter molecular CH– π interactions of $[Ce(BPBH)_2(NO_3)_3]$

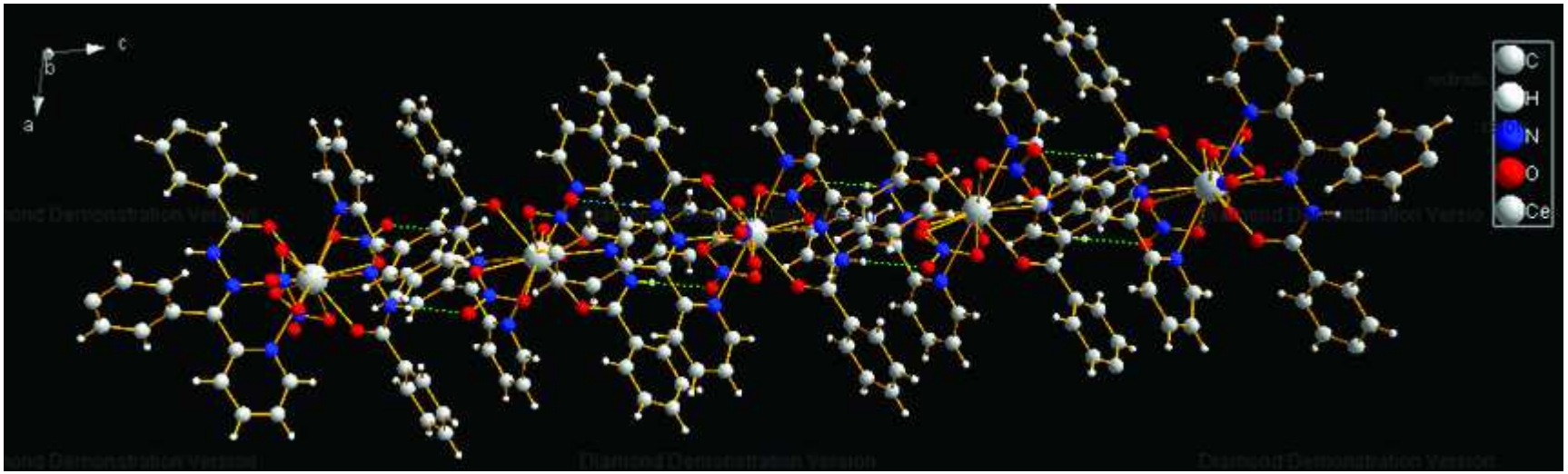

Fig 8.13: View of the Hydrogen bond (green dotted line) network of $[Ce(BPBH)_2(NO_3)_3]$

g. Hirshfeld surface analysis

The Hirshfeld surfaces represented by d_{norm} range of red (distances shorter than sum of vdW radii) through white to blue (distances longer than sum of vdW radii), shape index range of -1.0 (concave) through 0.0 (minimal surface) to +1.0 (convex), curvedness range of -4.0 (flat) through 0.0 (unit sphere) to +0.4 (singular), and 2-D fingerprint plots were calculated using Crystal Explorer 3.1 [16].

For each point on the Hirshfeld surface, two parameters are defined: d_e from the point to the nearest nucleus external to the surface and d_i is the distance from the point to the nearest nucleus internal to the surface. The normalized contact distance, dnorm, based on both de and di, and the vdW radius of the atom, given by an equation:

$$d_{norm} = \frac{d_i - r_i^{Vdw}}{r_i^{Vdw}} + \frac{d_e - r_e^{Vdw}}{r_e^{Vdw}} \qquad ..(1)$$

The Hirshfeld surface mapped over dnorm displays the intermolecular NH…$O_{(nitrate)}$ interactions as bright red areas and on the dnorm surface, a light red colour is indicates $CH_{(phenyl/Pyridine)}$…$O_{(nitrate)}$ interactions in Cerium complex shown in Fig. 8.14.

In the 2-D fingerprint plots, two distinct spikes appear for O…C/C…O intermolecular interactions. The proportion of O…C/C…O interactions comprises 4.2 % of the total Hirshfeld surfaces for each molecule of Cerium complex. This region corresponds to $O_{(nitrate)}$…π interaction in the fingerprint plot in a characteristic manner.

This decomposition enables separation of contributions from different interaction types, which overlap in the full fingerprint plot. In the 2-D fingerprint plots, two distinct spikes appear for O…H/H…O intermolecular interactions. The proportion of

O…H/H…O interactions comprises 27.3% of the total Hirshfeld surfaces for each molecule of 2. The upper spike corresponding to the donor represents the O…H interactions (di = 0.9, de = 1.2 Å) and the lower spike being an acceptor represents the H…O interactions (de = 0.9, di = 1.2 Å in 2) in the fingerprint plot (Fig. 8.15). The decomposition of the fingerprint plot shows that C…H/H…C contacts comprise 19.9% of the total Hirshfeld surface area for Ce complex. The region corresponds to all C–H…C interactions of which C–H…π appears in the fingerprint plot in a characteristic manner.

Hirshfeld surface of Ce complex does not show adjacent red and blue triangles on the shape-index surfaces (Fig. 8.14). However some carbon carbon interactions are present which comprises 3.6% of the total Hirshfed surface area of molecule. The proportion of H…H interactions comprises 41.4 % in 2D Fingerprint plot.

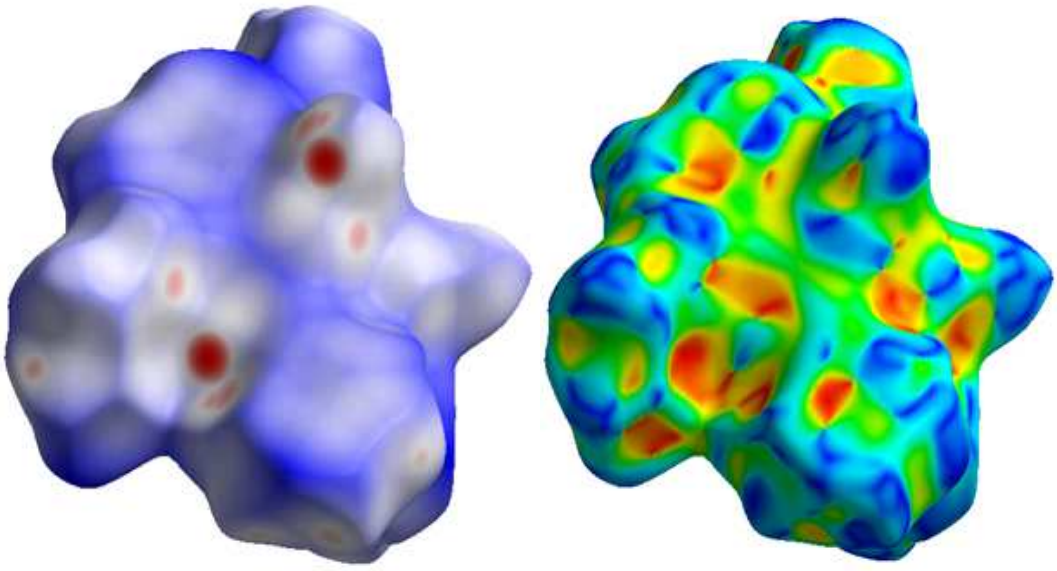

Fig 8.14: Hirshfeld surface mapped with (A) dnorm, (B) shape index for Ce complex

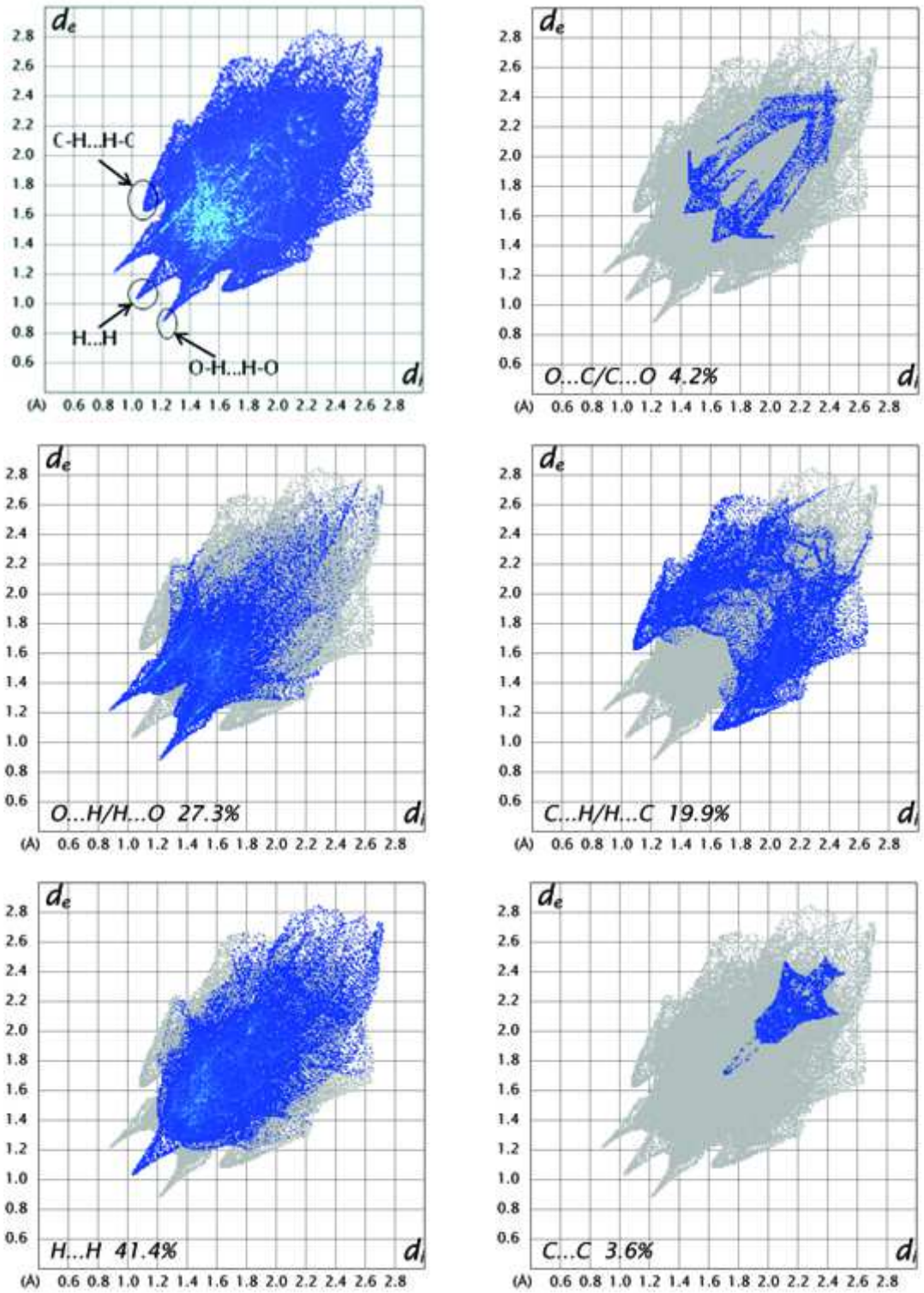

Fig 8.15: 2D fingerprint plots, full and resolved into OC/OC, OH/HO, CH/CH, H/H and C/C contacts showing percentages of contacts contributed to the total Hirshfeld surface area of molecule

h. Cyclic voltammetry

Redox behavior of the lanthanide(III) complexes has been investigated by cyclicvoltammetry using 0.1M tetrabutylammonium hexaflourophosphate (TBAHEP) as supporting electrolyte. The cyclicvoltammetric profiles of $[La(BPBH)_2(NO_3)_3]$ complex are given in Fig. 8.16. A plot of i_p vs $\upsilon^{1/2}$(scan rate) is linear (Fig. 8.17) pointing towards diffusion controlled nature of reduction wave. In the reverse scan there is no anodic peak confirming the irreversible nature of electrode process. All these facts pointed towards the diffusion-controlled nature of the electrode process.

The cyclic voltammograms of La(III), Ce(III). Pr(III), Nd(III) and Sm(III) gave irreversible waves. Their cathodic peak potentials are found to be -1.08 [La(III)], -1.35 [Ce(III)], -0.88 [Pr(III)], -1.0[Nd(III)] and -0.92[(Sm(III)] . This is due to the reduction of Ln(III) to Ln(II) couple [17].

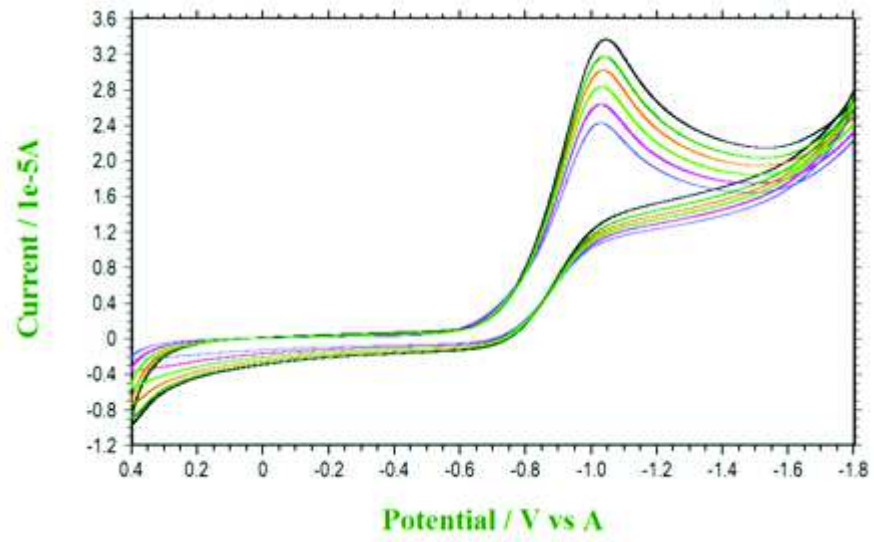

Fig 8.16: CV profiles of the Lanthanum complex at different scan rates 25-150 mV/s.

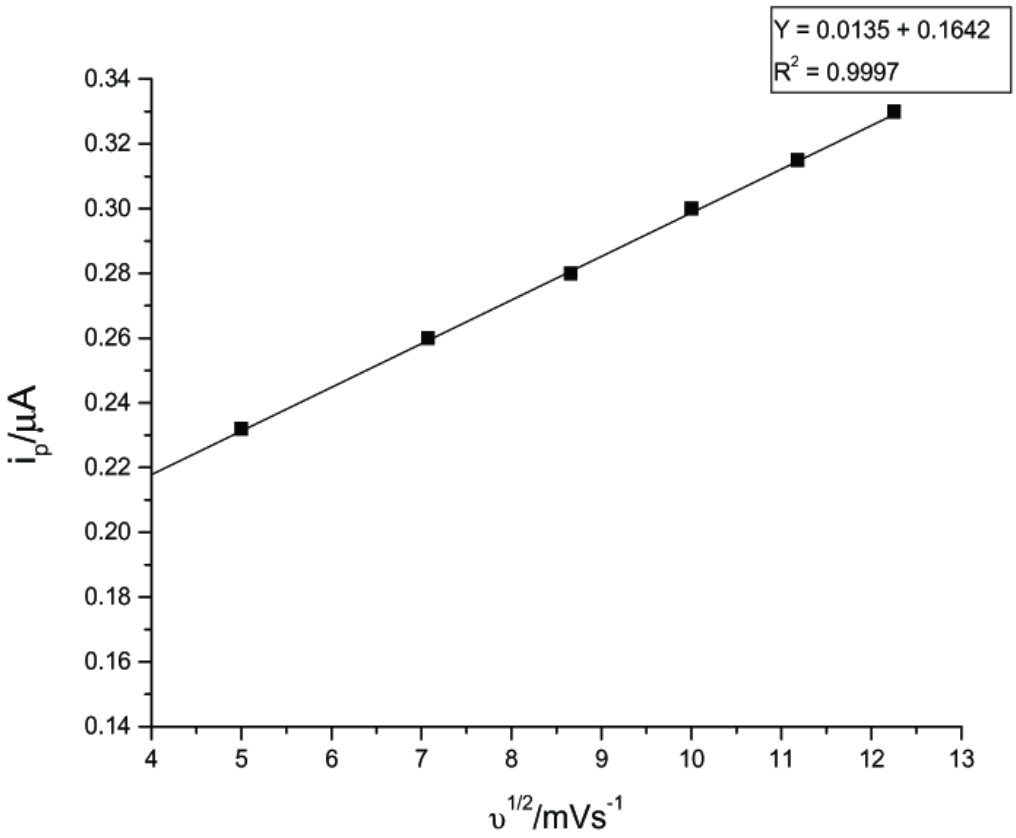

Fig 8.17: Plot of peak current vs scan rate for Lanthanum complex.

i. DNA binding studies

Electronic absorption spectroscopy is an effective method for examining the interaction of DNA with metal complexes. Hyperchromic and hypochromic effects are the spectral changes when a complex interacts with DNA and forms a new complex. In general, a complex binding with DNA through intercalation usually results in hypochromism and bathochromism of the absorption band due to the intercalative mode involving a strong π- stacking interaction between the aromatic chromophore and base pairs of DNA [18]. The binding interaction of complexes with CT-DNA was monitored by comparing their absorption spectra with and without CT-DNA. All the complexes exhibit an intense absorption band in 301-305 nm region

attributed to $\pi \rightarrow \pi^*$ transition. Absorption spectra of $[Ce(BPBH)_2(NO_3)(H_2O)_2].2NO_3.H_2O$ in the absence and in presence of CT-DNA are shown Fig. 8.18. The intrinsic binding constants (K_b), was determined by using the equation,

$$[DNA] / (\varepsilon_a - \varepsilon_f) = [DNA] / (\varepsilon_b - \varepsilon_f) + 1/ K_b(\varepsilon_b - \varepsilon_f) \quad \text{----------(1)}$$

Where [DNA] is the concentration of DNA in base pairs, ε_a, ε_b and ε_f are apparent extinction coefficient (A_{obs}/[M]), the extinction coefficient for the metal (M) complex in the fully bound form and the extinction coefficient for free metal (M) respectively. A plot of [DNA] / (ε_a-ε_f) versus [DNA] gave a slope of 1/(ε_b-ε_f), and vertical intercept equal to 1/ $K_b(\varepsilon_b - \varepsilon_f)$; K_b was calculated from these values. The binding constants (Table 8.8) for lanthanide complexes are almost similar and independent of metal ion. This observation suggests that the complexes do not bind DNA via coordination (No direct Metal- DNA bond formation). On addition of DNA, the absorbance of the complexes decreases (hypochromism). Negligible red shift(0.5-1.5 nm) in band position is observed for lanthanide complexes [19]. These observations suggest groove binding of complexes to DNA.

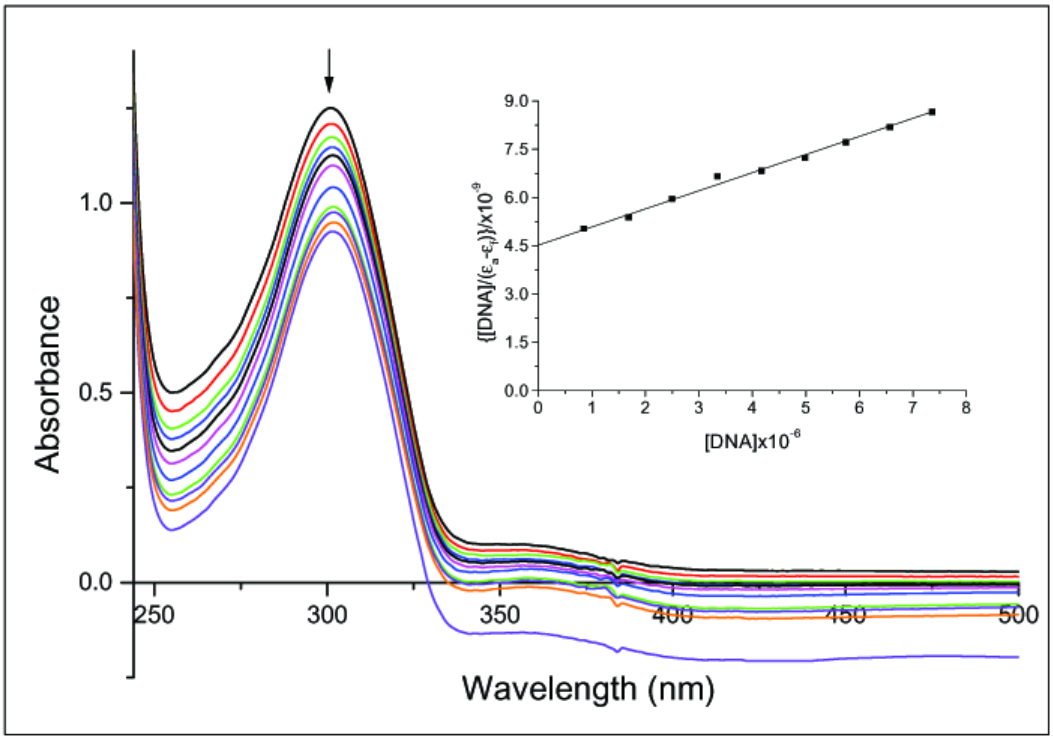

Fig 8.18: Absorption spectra of $[Ce(BPBH)_2(NO_3)_3]$ in the absence and in the presence of increasing concentration of CT-DNA; top most spectrum is recorded in the absence of DNA and below spectra on addition of 10 µl DNA each time.

Table 8.8. Electronic absorption data upon addition of CT-DNA to the complexes

Compound	**λ_{max} (nm)**		**Δλ**	**H(%)**	**K_b (M^{-1})**
	Free	**bound**			
$[La(BPBH)_2(NO_3)]$	301	302	1	+26.51	$1.87x10^5$
$[Ce(BPBH)_2(NO_3)]$	301	301.5	0.5	+27.32	$1.19x10^5$
$[Pr(BPBH)_2(NO_3)]$	300	301.5	1.5	+33.34	$1.94x10^5$
$[Nd(BPBH)_2(NO_3)]$	302	303	1	+30.47	$2.15x10^5$
$[Sm(BPBH)_2(NO_3)]$	304	305	1	+23.54	$2.01x10^5$

j. DNA Cleavage studies

Nuclease activity of lanthanide complexes with 2-benzoylpyridine benzoyl hydrazone (BPBH) has been studied by agarose gel electrophoresis using pBR 322 plasmid DNA in Tris-HCl/NaCl (50mM/5mM) buffer (pH-7) in the presence and in absence of H_2O_2 as an oxidant at micro molar concentration for 30 min incubation period at 37° C. In the presence of H_2O_2 the super coiled DNA (form I) is changed into nicked form (form II). Fig. 8.19 shows the cleavage activity of lanthanide complexes. In the presence of H_2O_2 the complexes cleave DNA more effectively [lanes 6, 8 and 10 in Fig.8.19], which may be due to the reaction of hydroxyl radical with DNA like Fenton mechanism [20]. These hydroxyl free radicals participate in the oxidation of the deoxyribose moiety [21]. The complexes may be arranged in the increasing order of nuclease activity (in the presence of hydrogen peroxide) as given below.

Ce complex > Pr complex > Nd complex > La complex

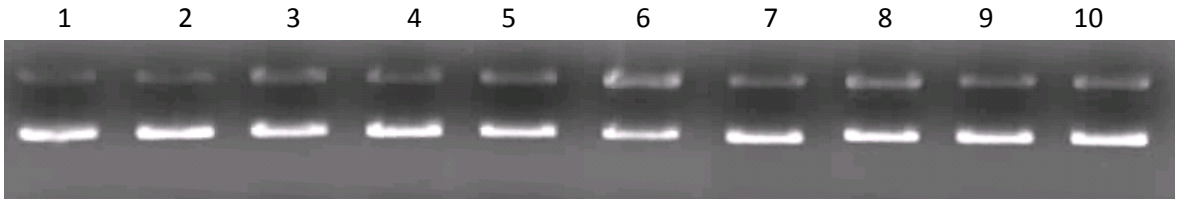

Fig 8.19: Agarose gel (0.8%) showing results of electrophoresis of 1 μl of pBR322 Plasmid DNA; 4 μl of Tris–HCl/NaCl (50 mM/5 mM) buffer (pH-7); 2 μl of complex in DMF($1x10^{-3}$ M); 11 μl of sterilized water; 2 μl of H_2O_2 (total volume 20 μl) were added, respectively, incubated at 37°C (30 min);

Lane 1: DNA control;
Lane 2: DNA control + H_2O_2;
Lane 3: Lanthanum complex+ DNA;
Lane 4: Lanthanum complex + DNA + H_2O_2;
Lane 5: Cerium complex+ DNA;
Lane 6: Cerium complex+ DNA + H_2O_2;
Lane 7: Praseodymium complex+ DNA;
Lane 8: Praseodymium complex+ DNA + H_2O_2;
Lane 9: Neodymium complex+ DNA;
Lane 10: Neodymium complex+ DNA+ H_2O_2.

Conclusions

Lanthanide(III) complexes of 2-benzoylpyridine benzhydrazone(BPBH) have been synthesized and characterized. Physico-chemical and spectral studies reveal that the complexes have general formula [Ln $(BPBH)_2$ $(NO_3)_3$] (where Ln = La, Ce, Pr, Nd, and Sm). BPBH acts as neutral tridentate ligand and NO_3^- acts as bidentate ligand. The structure of [$Ce(BPBH)_2(NO_3)_3$] complex is determined of single crystal X-ray diffraction studies. Two BPBH ligands occupy six coordination sites and three NO_3^- ligands another six coordination sites to form 12- coordinate mono nuclear

complexes. Absorption titrations suggest that the complexes bind DNA through intercalation involving a strong π -stacking interaction between the aromatic chromophore (pyridine moiety) and base pairs of DNA

The highlights of the present investigations (in this chapter) are: (i) The structures of the complex, $[Ce(BPBH)_2(NO_3)_3]$ is determined by single crystal X-Ray diffraction studies, (ii) Spectral and bonding parameters are calculated in support of covalent character of metal- ligand bond, (iii)Interactions of metal complexes with DNA are investigated using UV-Vis spectroscopy and (iv)Intercalative mode of binding of complexes to DNA is confirmed by viscosity measurements. .

Supplementary material

CCDC 917957 contains the supplementary crystallographic data for Ce complex. These data can be obtained free of charge via http://www.ccdc.cam.ac.uk/conts/retrieving.html, or from the Cambridge Crystallographic Data Centre, 12 Union Road, Cambridge CB2 1EZ, UK; fax: +44 1223 336 033; or e-mail: deposit@ccdc.cam.ac.uk.

References

1. E. Preshagen, E. Borbas, *Coord. Chem. Rev.* 273-274 **(2014)** 30.
2. C.M.G. Dos santos, J.H. Andrew, J.Q. Susan, T. Gunnlaugsson, *Coord. Chem. Rev.* 252 **(2008)** 2512.
3. B. Melanie, K. Lilan, J.L. Nicholas Chem. Soc. Rev. 35 **(2006)** 557.
4. C.A. Barta, S.B. Krishna, J. Jesica, K.H. Thomspon, M.W. Kishore, O. Chris *Dalton Trans.* **(2007)** 5019
5. W. J. Geary, *Coord. Chem. Rev.* 7 **(1971)** 81.
6. S.P. Sinha, *Spectrochim Acta* 22 **(1966)** 57.
7. K. Iftikar, M. Sayeed and N. Ahmad, *Bull. Chem. Soc. Japan* 55 **(1982)** 2258.
8. K. Nakamoto, Infrared and Raman Spectra of Inorganic and Coordination Compounds, fourth ed., Wiley, New York, 1986.
9. N.F. Curtis, Y.M. Curtis, *Inorg. Chem.* 4 **(1965)** 804.
10. P. Yan, W. Sun, G. Li, C. Nei, T. Gao, Z. Yue, *J. Coord. Chem.* 60 **(2007)** 1973.
11. X.M. Shi, R.R. Tang, G.L. Gu, K.L. Huang, *Spectrochim. Acta* 72A **(2009)** 198.
12. S.P. SINHA, *Systematics and the properties of lanthanides, NATO ASI Series, Series C. Mathematical and Physical Sciences* No.109, p131 **(1982)**
13. M.Carcelli, S.Ianelli, P.Pelagatti, G.Pelizzi, D.Rogolino, C.Solinas, M.Tegoni, *Inorg. Chim. Acta.* 358 **(2005)** 903.
14. J. Dan, S. Seth, S. Chakraborty, *Acta. Crystllogr. Sect. C* 45 **(1988)** 1018.
15. P. Sathyadevi, P. Krishnamoorthy, M. Alagesan, K. Thanigaimani, P.T. Muthiah , N. Dharmaraj, *Polyhedron* 31 **(2012)** 294.
16. S.K. Wolff, D.J. Grimwood, J.J. McKinnon, M.J. Turner, D. Jayatilaka, M.A. Spackman, University of Western Australia, 2012.

17. Ch. Jagadeeswara Rao, K.A. Venkatesan, K. Nagarajan, T.G. Srinivasan, P.R. Vasudeva Rao, *J. Nucl. Mater.* 399 **(2010)** 81.

18. E.C. Long, J.K. Barton, *Acc. Chem. Soc. Res.* 23 **(1990)** 271.

19. S. Ramakrishnan, E Suresh, A. Riyasdeen, M. A. Akbarsha, M. Palaniandavar. *Dalton Trans.* 40 **(2011)** 3245.

20. Y.M. Song, J.P. Xu, L. Ding, Q. Hou, J.W. Liu, Z.L. Zhu, *J. Inorg. Biochem.* 103 **(2005)** 396.

21. W.K. Pogozelski, T.D. Tullius, *Chem. Rev.* 98 **(1998)** 1089.